Current Research in Structural Biology 7 (2024) 100149

Contents lists available at ScienceDirect

Current Research in Structural Biology

journal homepage: www.journals.elsevier.com/current-research-in-structural-biology

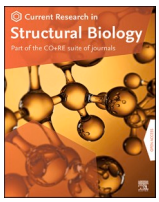

Research Article

Membrane binding and lipid-protein interaction of the C2 domain from coagulation factor V

Y. Zenmei Ohkubo [a], Peter W. Radulovic [b,1], Albert N. Kahira [c,2], Jesper J. Madsen [d,e,*]

[a] Department of Bioinformatics, School of Life and Natural Sciences, Abdullah Gül University, Kayseri, Turkey
[b] Graduate Programs, Taneja College of Pharmacy, University of South Florida, Tampa, FL 33612, USA
[c] Graduate Programs, School of Engineering, Abdullah Gül University, Kayseri, Turkey
[d] Department of Molecular Medicine, Morsani College of Medicine, University of South Florida, Tampa, FL 33612, USA
[e] Center for Global Health and Infectious Diseases Research, Global and Planetary Health, College of Public Health, University of South Florida, Tampa, FL 33612, USA

ARTICLE INFO

Handling editor: Dr A Wlodawer

Keywords:
C2 domain
Coagulation factors
Factor V
Membrane anchoring
Lipid-protein interaction
Anionic lipids
HMMM model
Molecular dynamics simulation

ABSTRACT

Anchoring of coagulation factors to anionic regions of the membrane involves the C2 domain as a key player. The rate of enzymatic reactions of the coagulation factors is increased by several orders of magnitude upon membrane binding. However, the precise mechanisms behind the rate acceleration remain unclear, primarily because of a lack of understanding of the conformational dynamics of the C2-containing factors and corresponding complexes. We elucidate the membrane-bound form of the C2 domain from human coagulation factor V (FV–C2) by characterizing its membrane binding the specific lipid-protein interactions. Employing all-atom molecular dynamics simulations and leveraging the highly mobile membrane-mimetic (HMMM) model, we observed spontaneous binding of FV-C2 to a phosphatidylserine (PS)-containing membrane within 2–25 ns across twelve independent simulations. FV-C2 interacted with the membrane through three loops (spikes 1–3), achieving a converged, stable orientation. Multiple HMMM trajectories of the spontaneous membrane binding provided extensive sampling and ample data to examine the membrane-induced effects on the conformational dynamics of C2 as well as specific lipid-protein interactions. Despite existing crystal structures representing presumed "open" and "closed" states of FV-C2, our results revealed a continuous distribution of structures between these states, with the most populated structures differing from both "open" and "closed" states observed in crystal environments. Lastly, we characterized a putative PS-specific binding site formed by K23, Q48, and S78 located in the groove enclosed by spikes 1–3 (PS-specificity pocket), suggesting a different orientation of a bound headgroup moiety compared to previous proposals based upon analysis of static crystal structures.

1. Introduction

Coagulation factors employ two structurally distinct membrane binding domains; the enzymes often feature GLA domains, while the cofactors include the C2-like domains (Pellequer et al., 1998; Zwaal et al., 1998; Pellequer et al., 2000; Lemmon, 2008). Factor V (FV) and factor VIII (FVIII, denoted similarly for other factors in subsequent acronyms) use the C1 and C2 domains (both C2-like) to anchor themselves to anionic membranes, notably those containing phosphatidylserine lipids (Villoutreix et al., 1998; Macedo-Ribeiro et al., 1999; Pratt et al., 1999; Adams et al., 2004; Stace and Ktistakis, 2006, Ngo et al., 2008; Antila et al., 2019). The C1 and C2 domains are members of the discoidin domain family (Baumgartner et al., 1998; Stace and Ktistakis, 2006; Lemmon, 2008) and are also found in other membrane-binding proteins such as lactadherin (Lin et al., 2007; Shao et al., 2008). It's important to note that these discoidin-type C2 domains are unrelated (Nalefski and Falke, 1996; Rizo and Südhof, 1998; Lemmon, 2008) to the C2 domains of protein kinase Cα (Verdaguer et al., 1999) and cytosolic phospholipase A2 (Perisic et al., 1998). Establishing structural models of membrane-bound C2-domain-containing proteins is crucial for understanding the molecular mechanisms underlying the enzymatic activities of prothrombinase (PTase; a complex of FVa:FXa; "a" denoting "activated") and the intrinsic FXase (FVIIIa:FIXa) complexes on the physiologically relevant membrane surfaces, including the activated

* Corresponding author. Department of Molecular Medicine, Morsani College of Medicine, University of South Florida, Tampa, FL 33612, USA.
E-mail address: jespermadsen@usf.edu (J.J. Madsen).
[1] Current affiliation: H. Lee Moffitt Cancer Center & Research Institute, Tampa, FL 33612, USA.
[2] Current affiliation: Jülich Supercomputing Center, 52,428 Jülich, Germany.

https://doi.org/10.1016/j.crstbi.2024.100149
Received 23 November 2023; Received in revised form 28 March 2024; Accepted 29 April 2024
Available online 1 May 2024

platelets (Bos and Camire, 2010; Rietveld et al., 2018; Schreuder et al., 2019; Ohkubo and Madsen, 2021).

The C2 domain is structurally very different from the GLA domains. It contains an eight-stranded Greek-key motif β-barrel with three putative membrane-binding loops, termed Spikes 1, 2, and 3 (S1, S2, and S3) (Macedo-Ribeiro et al., 1999) (Fig. 1). Furthermore, the C2 domain does not include post-translationally modified γ-carboxyglutamate residues and thus lacks specific Ca^{2+}-binding sites crucial for the folding and membrane binding observed in GLA domains interacting with anionic lipids (Sunnerhagen et al., 1995; Ohkubo and Tajkhorshid, 2008). Two distinct structures of the human FV-C2 domain (hFV-C2) have been resolved with X-ray crystallography: the "open" (PDB entries 1CZS and 1CZT) and the "closed" forms (1CZV) (Macedo-Ribeiro et al., 1999). Their main distinction is the conformation of S1 and the orientations of two potential membrane-binding residues, W26 and W27, in S1 (Fig. 1). Although it has been proposed that the "closed" and "open" forms may represent solution and membrane-bound states, respectively, with their interconversion being a crucial step in the C2 domain anchoring process (Macedo-Ribeiro et al., 1999), there is currently no empirical evidence supporting this hypothesis aside from simulation studies (Mollica et al., 2006; Wu et al., 2009). Wu et al. used implicit membrane models to identify a barrier between the "open" and "closed" forms that is easily crossable (~1.5 kcal/mol) (Wu et al., 2009). Mollica et al. conducted relatively brief simulations in water and while bound to a membrane patch of 1-palmitoyl-2-oleyl-phosphatidylethanolamine (POPE) to investigate the transition from "open" to "closed" C2 (Mollica et al., 2006). However, the existence of the two conformational states of C2 and their potential relevance to membrane binding and lipid interaction remain open questions. Furthermore, the selection of lipid conformation can also come into play (Bacle et al., 2021), adding a potential layer of complexity.

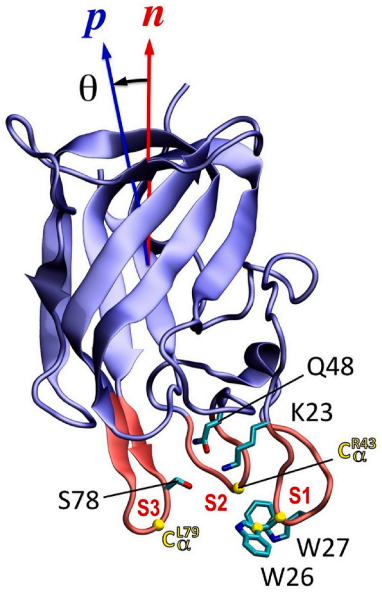

Fig. 1. Structure of the C2 domain from factor V (FV–C2). The mainchain is shown in blue cartoon representation, with the membrane binding loops, Spikes 1, 2, and 3 highlighted in red and labeled "S1", "S2", and "S3", respectively. The sidechains of W26 and W27 on S1 are drawn in licorice representation. The sidechains of K23, Q48 and S78, which have been suggested to form the putative PS-specificity pocket (Macedo-Ribeiro et al., 1999), are also shown in licorice. The atoms used for measuring the inter-spike distances and the orientation of W26 sidechain (Cα atoms of W26, R43 and, L79; Cγ of W26) are indicated by yellow spheres. To monitor the relative orientation of the C2 domain with respect to the membrane, the tilt angle of FV-C2, θ, is defined as the angle between the membrane normal (red arrow mark with "*n*") and the first principal axis of the C2 domain (blue arrow labeled "*p*").

In addition to hFV-C2, several structures of the C2 domain of hFVIII (FVIII–C2) have also been solved (PDB entries 1D7P (Pratt et al., 1999), 1IQD (Spiegel et al., 2001), 3CDZ (Ngo et al., 2008), 2R7E (Shen et al., 2008)). In contrast to FV-C2, the structures available for FVIII-C2 do not support the existence of two distinct ("open" and "closed") conformations. The C1 domain, situated on the N-terminal side of the C2 domain in the light chain of both FV and FVIII, is highly homologous to and shares a common topology with the C2 domain (Fig. 2). Structural insights into the C1 domains are derived from hFVa (PDB entry 1FV4 (Pellequer et al., 2000)), protein C-inactivated bovine FVa (bFVai; PDB 1SDD (Adams et al., 2004)), and hFVIII (3CDZ (Ngo et al., 2008); 2R7E (Shen et al., 2008); 4BDV (Svensson et al., 2013)). More recently, structures have appeared even of complexes containing the full coagulation factors (Lechtenberg et al., 2013; Ruben et al., 2021; Di Cera et al., 2022; Ruben et al., 2022; Mohammed et al., 2023).

There is accumulating evidence supporting the involvement of the C1 and C2 domains in membrane binding of FV and FVIII (Macedo-Ribeiro et al., 1999; Srivastava et al., 2001; Spiegel et al., 2004; Segers et al., 2007). It was shown that the C1 and C2 domains include PS binding sites that are important for membrane binding of FVa (Majumder et al., 2005; Majumder et al., 2008) and that the C1 domain also regulates assembly of the FVa:FXa complex (Majumder et al., 2008). In another study, deletion of the C2 domain from FV was reported to result in complete loss of PS-specific binding (Ortel et al., 1992a). Moreover, immunoglobulins, known to bind FV-C2, have an inhibitory effect on the PTase activity, probably by diminishing the binding of FVa to PS-containing membranes (Ortel et al., 1992b). Furthermore, mutagenesis studies imply a direct role of S1 of FV-C2 in binding to PS-containing membranes (Nicolaes et al., 2000).

We use MD simulations to elucidate membrane binding and the membrane-bound forms of the FV-C2 domain to anionic membranes. This methodology facilitates a detailed investigation on the atomic level into the orientation and insertion depth of membrane-bound C2 as well as identification of the specific sidechain–PS headgroup interactions. Because of its augmented lipid mobility, the HMMM model (Ohkubo et al., 2012; Vermaas et al., 2015; Baylon et al., 2016) is an ideal tool for this purpose.

2. Methods

2.1. Structures of the C2 domain from human FV

The X-ray structures of the C2 domain from the PDB entries 1CZS ("open" form) and the chain A of 1CZV ("closed") (Macedo-Ribeiro et al., 1999) were used for the initial conformations of the systems simulated in this study, to investigate whether the X-ray "open" and "closed" structures represent either membrane-bound or solution forms of the C2 domain. Hydrogen atoms were added and the N- and C-termini were patched with charged amino and carboxy groups, respectively.

2.2. HMMM model

The highly mobile membrane-mimetic (HMMM) model (Ohkubo et al., 2012) was employed to expedite the formation and convergence of lipid-protein interactions. The HMMM-based membrane used was composed of 1,1-dichloroethane (DCE) molecules, representing the hydrophobic core, and short-tailed lipid (divalerylphosphatidylserine, DVPS) molecules for phosphatidylserine (PS) lipids (Arcario et al., 2011; Ohkubo et al., 2012; Vermaas et al., 2017). The HMMM patch size (i.e., the *x-y* dimensions of the unit cell) was 90×90 Å^2 with 128 DVPS molecules (64 lipids in each leaflet) included. The resulting area per lipid is 127 Å^2, which is about twice as large as an experimentally obtained number (Petrache et al., 2004), allowing for nearly two orders of magnitude enhancement in lateral diffusion of DVPS while the membrane profile remains fairly unchanged with minimal occurrence and

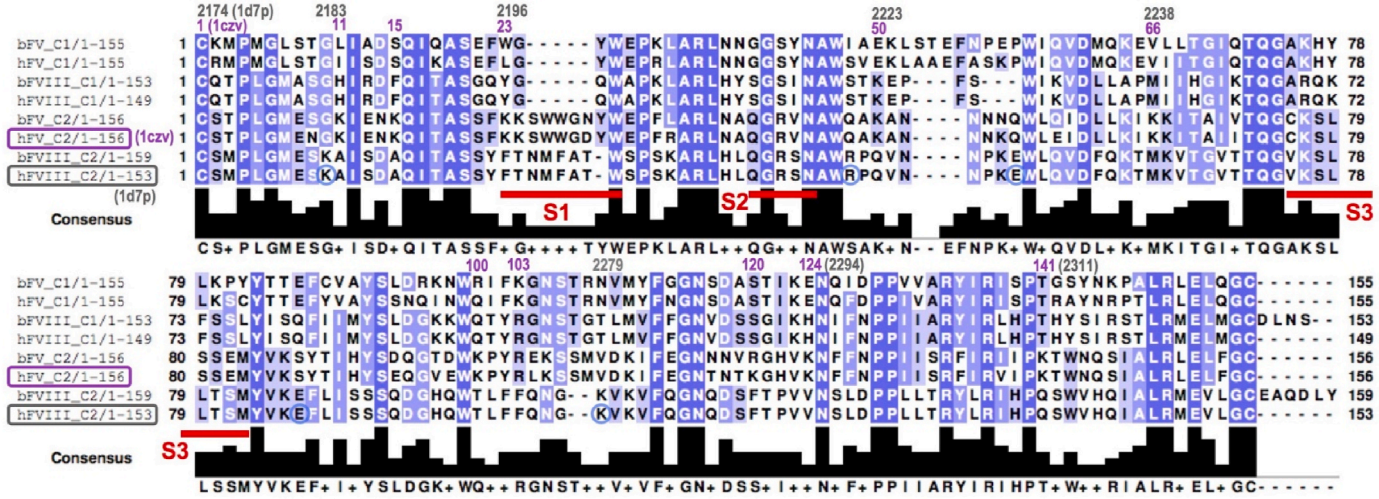

Fig. 2. Sequence alignment of the C1 and C2 domains. The sequences of the C1 and C2 domains from human or bovine FV and FVIII are aligned using ClustalW2 (Larkin et al., 2007). The positions of S1, S2, and S3 of hFV-C2 are indicated by red bars.

influence of water penetration into the membrane or DCE solvent ejection (Ohkubo et al., 2012; Vermaas et al., 2017). Lipid-protein interactions are expected to be rather independent to the lipid density of the HMMM because the headgroup-involved interactions are mostly long-range electrostatic (Antila et al., 2019; Kiirikki et al., 2024), and therefore the lipids move around and can gather around FV-C2. For hydrophobic interactions, not only the acyl tails of the lipids but also the bulk DCE molecules, are expected to be involved. The membrane thickness, measured by the phosphate–phosphate distance (D_{P-P}), was set at ~40 Å (Fig. 3). Improved methodology for the HMMM membrane patch such as the extended HMMM (*ext*HMMM) recently proposed (Ohkubo and Madsen, 2023) was found unnecessary due to the relatively small size of a system containing the C2 domain.

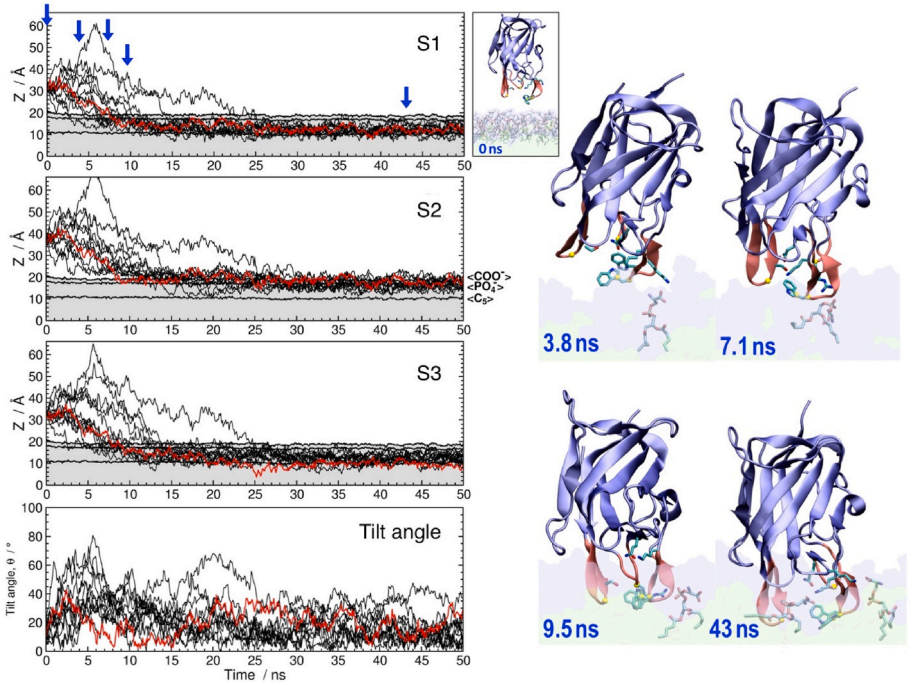

Fig. 3. A converged membrane binding of FV-C2 depicted by the height of S1-3 and the tilt angle, θ. The left side panels show the twelve membrane simulations, the height of the tips of S1, S2, and S3 from the membrane center as well as θ are plotted in black lines (except for one shown in red, highlighted for more detailed exploration on the right) as a function of MD simulation time (left side panels). The spike tips are defined as the midpoint of Cα atoms of W26 and W27 (S1), Cα atom of R43 (S2), and the midpoint of Cα atoms of L79 and S80 (S3). The membrane center is defined as the center of mass of DCE molecules. The average heights for the membrane components shown in the panels are from a single set for clarity; the means and deviations of the heights are very close from set to set. The gray zones in the top three panels represent the membrane layer, and three horizontal lines in the zone indicate the average heights of the carboxy carbons, phosphorus atoms, and the carbons at the acyl tail ends (labeled <COO−>, <PO4−>, and <C5>, respectively). A typical trajectory is highlighted in red lines with its closed-up snapshots of the C2 domain on the right side. The instantaneous times are labeled on the snapshots and are also indicated as blue arrows in the S1 plot. The initial (0 ns) configuration is in an inset and is aligned to the S1 panel with the matching scale.

2.3. Simulation procedures

All-atom MD simulations were performed using NAMD2 (Phillips et al., 2005), with the CHARMM27 force field parameters (MacKerell et al., 1998) in conjunction with the CMAP corrections (Mackerell et al., 2004) for proteins and the CHARMM36 force field parameters (Vanommeslaeghe et al., 2010) for lipids. The membrane-binding systems were simulated in the NP_nAT ensemble, and the solution systems in the *NPT* ensemble. Explicit TIP3P water molecules (Jorgensen et al., 1983) were used for all simulations. The target temperature was set at 310 K and maintained by using Langevin dynamics with a damping coefficient of 0.5 ps^{-1}. The pressure was maintained at 1 atm by Langevin piston Nosé-Hoover method (Martyna et al., 1994; Feller et al., 1995). The long-range electrostatic forces were computed without truncation using the particle mesh Ewald (PME) method (Darden et al., 1993; Essmann et al., 1995) with a grid density of ~ 1 $Å^{-3}$. Integration time steps for bonded, nonbonded, and PME calculation were set to 2, 2, and 4 fs, respectively. The cut-off for the van der Waals interaction was set at 12.0 Å.

2.4. Membrane binding simulations of the C2 domain

Simulations for membrane binding of FV-C2 were performed to obtain the membrane-bound form of FV-C2 and specific lipid-protein interactions. A $90 \times 90 \times 30$ (along the x, y and z axis, respectively) $Å^3$ volume of DCE was prepared and then padded with 65 Å- and 35 Å-thick water slabs on positive and negative z side. Subsequently, 64 DVPS lipids were added with the phosphorus atoms at around the DCE–water interface and acyl tails in DCE region for each interface. The "closed" (1CZV) structure was placed in the thicker water layer ~ 10 Å above the membrane surface with the membrane-binding spikes facing the membrane (Fig. 3, inset "0 ns"). Water and DCE molecules that overlapped with the lipids or the protein were removed, and the system was then neutralized with Na^+ ions. The monovalent cation was chosen as counterions instead of Ca^{2+} to minimize cation-mediated lipid–lipid interactions (Boettcher et al., 2011), which gives larger lateral mobility to the lipids (Ohkubo et al., 2012) and increases chances of lipid–protein interactions. The neutralized systems were then energy-minimized by 1000 steps of a conjugate gradient method (Hestenes and Stiefel, 1952), heated to 310 K in 500 steps, relaxed for 3000 steps at 310 K, while fixing the position of the Cα atoms of the C2 domain in order to sustain the C2-membrane distance. Subsequently, the system was relaxed for another 3000 steps without any restraint on the C2 domain. The 50-ns-long NP_nAT simulations were performed twelve times, ensuring good sampling and convergence of computed properties (Table 1).

2.5. Solution simulation of the C2 domain

Simulations for the C2 domain in solution were performed to investigate whether either the "open" (PDB 1CZS) or "closed" (1CZV) form represents the solution structure of the C2 domain. A system including a single FV-C2 molecule was prepared for each form using the same following procedures. The proteins were solvated in a water box that provided a minimum padding of 12 Å on each side, resulting in approximately $67 \times 67 \times 87$ $Å^3$ unit cells. The systems were then neutralized by randomly replacing water molecules in the bulk with Ca^{2+} and Cl^- ions (the net ion concentration is 0.19 M). While monovalent cations were used as counterions in the membrane-binding simulation to sustain high lateral mobility of HMMM-forming lipids, divalent Ca^{2+} ions were used here to minimize the number of counterions in the system. Influence of different cation types over the structure and dynamics of FV-C2 are negligible. The solvated and neutralized systems were then energy-minimized by 1000 steps of the conjugate gradient method (Hestenes and Stiefel, 1952), while weakly restraining the Cα atoms of the C2 domain to the original positions with the spring constant of 29 kJ mol^{-1} $Å^{-}1$ (7.0 kcal/mol $Å^{-1}$) in order to sustain the orientation of the domain in the system. Subsequently, the production MD simulations were performed in *NPT* ensemble for 100 ns? Systems with C2 in water only are substantially easier to converge, and thus more replicas were performed for the membrane-containing systems (Table 1).

Table 1
Systems simulated in the present study. Both the membrane and solution systems contain a copy of the C2 domain of human factor V (FV–C2), whose initial structure is either from PDB 1CZS ("open") or 1CZV ("closed").

System	Unit cell size $x \times y \times z$ / $Å^3$	Init. Structure of C2 domain	Number of simulations	Simulation length/ns
Membrane	$90 \times 90 \times \sim 128$	"closed"	12	50
Solution	$\sim 67 \times \sim 76 \times \sim 87$	"closed"	1	100
Solution	$\sim 67 \times \sim 76 \times \sim 87$	"open"	2	100

2.6. AlphaFold2 predictions

Prediction of a structural ensemble for hFV-C2 was performed with AlphaFold2 (Jumper et al., 2021) using ColabFold (Mirdita et al., 2022) and MMseqs2 (Steinegger and Soding, 2017). 16 different seeds were used to make 5 models each, giving 80 models in total.

3. Results & discussion

A summary of the findings is as follows, with further elaboration and specific information provided in subsequent sections. Employing the HMMM model of anionic membranes allowed for determining the membrane-bound form of FV-C2. Multiple, relatively short molecular dynamics (MD) simulations of a system that include a HMMM-based pure-PS membrane captured the spontaneous membrane binding of FV-C2 repeatedly, providing enhanced statistics on specific lipid-protein interactions. FV-C2 bound to the PS membrane at S1, S2 and S3 with its β-barrel nearly aligned with the membrane normal as previously postulated (Macedo-Ribeiro et al., 1999; Adams et al., 2004; Peng et al., 2005; Mollica et al., 2006; Stoilova-Mcphie et al., 2008). Spikes S1 and S3 did not exhibit significant backbone perturbations upon membrane binding, while the sidechain of W26 in S1 changed its orientation. A PS lipid bound to the PS-specificity pocket (Macedo-Ribeiro et al., 1999) consistently. Simulations conducted in bulk water for FV-C2, initiated from either the "open" or "closed" forms, sampled overlapping conformational ensembles, i.e., there was no observed dependence on the choice of the initial structure.

3.1. Converged membrane-binding orientation of the C2 domain

To explore the membrane-bound form of the C2 domain of human FV (hFV-C2), twelve sets of 50-ns-long MD simulations were performed. The system simulated consisted of a pure divalerylphosphatidylserine (DVPS) HMMM-based membrane and a single FV-C2 (from PDB 1CZV) initially placed in the bulk water (Fig. 1).

In all cases, FV-C2 spontaneously bound to the membrane at putative membrane-binding regions, namely Spikes 1, 2 and 3 (S1, S2 and S3) (Macedo-Ribeiro et al., 1999). The three spikes were inserted into the membrane within 2–25ns, after which the spike tips reached asymptotic heights from the membrane center (Fig. 3). The tips of S1 and S3 reached the acyl tail region (Fig. 3), i.e., the layer between the average height from the membrane center for phosphorus atoms (<PO4−>) and that for the carbons at the acyl tail end (<C5>). The tip of S2, which is shorter than S1 and S3, on the other hand, fluctuates around the headgroup layer (between <COO−> and <PO4−> in Fig. 3). The β-barrel of

FV-C2 is almost perpendicular to the membrane surface when all spikes are inserted in the membrane (Fig. 3, "9.5 ns" when all spikes were first inserted, and "43 ns" after well-equilibrated).

The orientation of FV-C2, represented by the tilt angle of the first principal axis of the protein from the membrane normal (Fig. 1), converged into a narrower range of 10–30°, after S1–S3 were fully buried into the membrane (Fig. 3). For comparison, the tilt angle varied from 0° to 80° beforehand, due to free rotation of the protein in the bulk water. The tilt angle of 10–30° means that the β-barrel is nearly vertical to the membrane in the obtained membrane-bound form of FV-C2 (Fig. 3), which is similar to the PS-containing lipid tube-bound model for the entire FVa based on electron microscopy data ("FVaEM" model) (Stoilova-Mcphie et al., 2008). In the FVaEM model, however, the insertion depth of C2 domain is around 20 Å, while in our HMMM-bound model, S1 and S3 are inserted into the membrane around 10 Å below the membrane surface represented by <COO−> (Fig. 3). We have

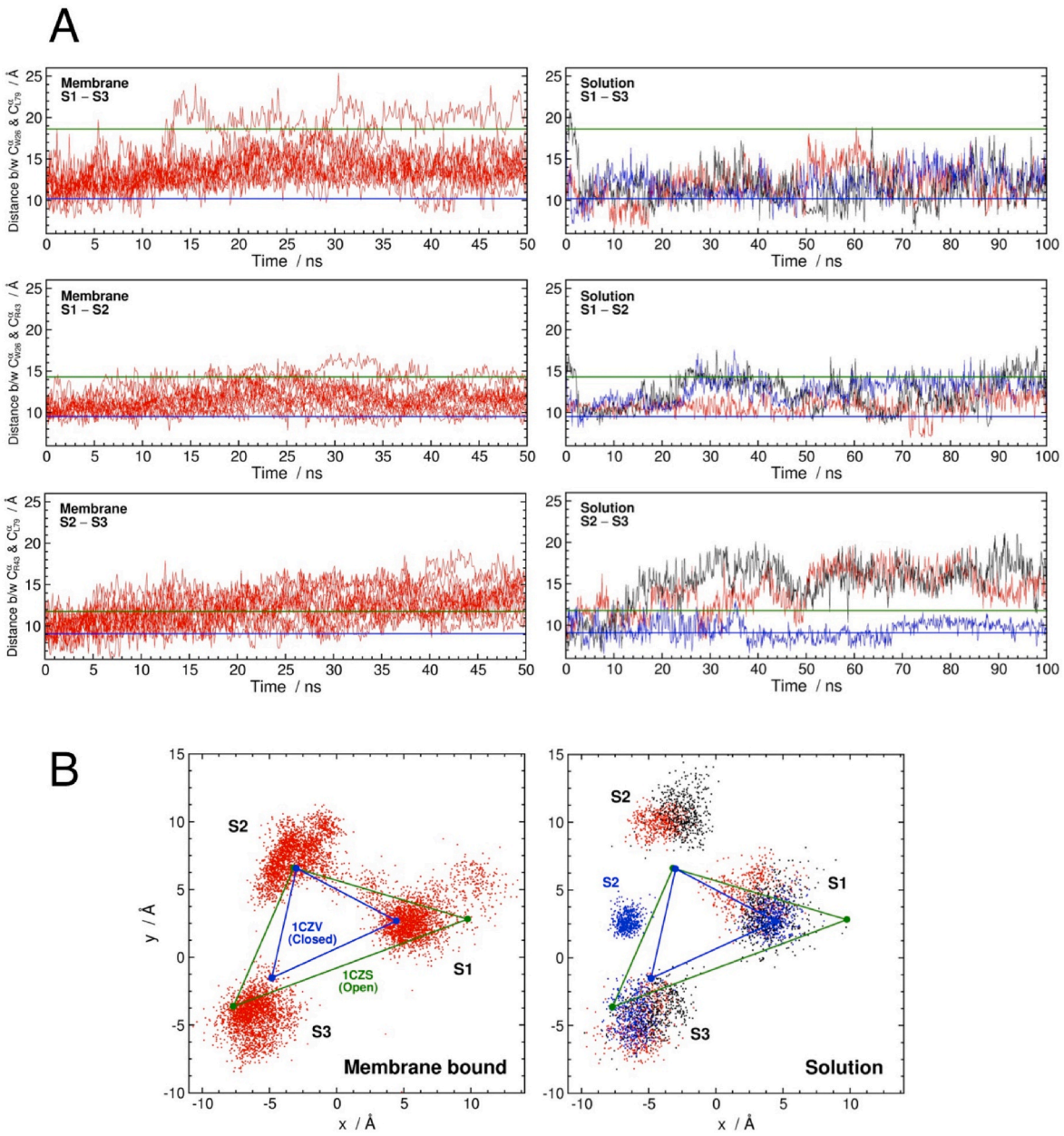

Fig. 4. Distances between S1, S2, and S3 during the membrane-binding (left panels) and solution (right) simulation of the C2 domain. (**A**) The distances between the tips of S1, S2, and S3 (see Fig. 3 legend) measured every 0.1 ns are plotted as a function of time. The horizontal lines indicate the tip-tip distances in two X-ray structures, 1CZV "closed" (in blue) and 1CZS "open" (green) (Macedo-Ribeiro et al., 1999), respectively. Note the different time scales for the membrane and solution simulations. Data from solutions simulations are colored as differently for the three simulations ("closed" in black and the two "open" trajectories in red and blue). (**B**) Fluctuation of tips of S1–3 during the membrane-binding and solution simulation. The *(x, y)* coordinates of the tips of S1, S2, and S3 (represented by the Cα atoms of W26, R43, and L79, respectively) are depicted for superimposed structures from every 0.1 ns of the last 20 ns (membrane-binding) or 50 ns (solution) of simulations. The reference for the superimposition is the chain A of PDB 1CZV (Macedo-Ribeiro et al., 1999), with its center of mass was matched to the origin and the first, second, and third principal axes aligned with the *z*, *x*, and *y* axes, respectively (note that the *z* axis is the membrane normal in all simulations). Subsequently, the superimposition was performed by aligning the instantaneous structures onto the reference, using the Cα carbons in relatively stable β strands (*i.e.*, residues 13–20, 32–36, 57–61, 70–75, 85–93, 113–117, 123–127, 135–139 and 150–154). The 1CZS "open" structure is also superimposed in the same manner. The tip positions of the two X-ray structures are indicated by large blue (for 1CZV) or green (1CZS) spheres connected by lines in the same colors. Data from solutions simulations are colored as differently for the three simulations ("closed" in black and the two "open" trajectories in red and blue).

previously speculated that this difference can be attributed to the relatively high curvature of the lipid nanotubes employed to secure FVa in the FVaEM structure (Ohkubo and Madsen, 2021), and this remains our interpretation.

3.2. Interplay between the X-ray, membrane-bound, and solution structures of FV-C2

There are two X-ray solved, distinguishable structures for FV-C2: 1CZS and 1CZV, referred to as "open" and "closed" forms, respectively, due to the differences in the conformation of S1 (Macedo-Ribeiro et al., 1999) and the orientation of the sidechains of the S1 sidechain W26 and W27 conformations (Fig. 1). It has been suggested that the X-ray "open" and "closed" forms might represent membrane-free and membrane-bound forms (Macedo-Ribeiro et al., 1999), which is supported in part by MD simulations of FV-C2 binding to neutral POPE membranes (Mollica et al., 2006). Through, it cannot be ruled out that the differences arise from varying crystallization conditions.

The two structures were, however, not observed as clearly distinct forms during the membrane-binding or solution simulations of FV-C2, as found by monitoring the distance between the S1 Cα atom of W26 and that of L79 on S3 (Fig. 4). In all except one case (which will be mentioned later) of the membrane-binding simulations, the S1–S3 distance (distance between S1 and S3) converged to a value between those for the X-ray "open" (18.6 Å, shown as green horizontal lines) and "closed" (10.2 Å, blue lines) structures, ranging mostly from 11 to 16 Å (Fig. 4A). In the case of solution simulations, the S1–S3 distance exhibited a similar behavior to the membrane-binding simulations, i.e., mostly ranging from 9 to 15 Å and seldom exceeding 16 Å, regardless of the initial structure (Fig. 4A).

Similar trends were observed for two other inter-spike distances in the membrane-binding simulation. The S1–S2 distance fluctuated mostly between the "closed" distance (9.5 Å) and the "open" (14.3 Å) before and after membrane binding. The S2–S3 distance increased slightly over time and then fluctuated around or above the "open" distance (11.8 Å) after membrane binding, yet it occasionally visited the neighborhood of the "closed" distance (9.1 Å) (Fig. 4A). As for the solution simulations, on the other hand, the S2–S3 distance exceeded the "open" distance (14.3 Å) in two trajectories and remained around the "closed" (9.5 Å) in the rest, implying that the conformation of S2 is different from that in the membrane-bound form. One contributing factor may be the comparatively shorter length of S2 compared to S1 and S3, a characteristic that aligns with its smaller insertion depth.

Therefore, no clear transition from the "closed" to the "open" upon the membrane binding was observed. Both X-ray "closed" and "open" structures were visited as membrane-bound states occasionally, but not well populated. In solution, S2 seems to exhibit two conformations that are different from the X-ray structures.

The relative fluctuation of the tip positions of S1–S3 during the simulations are depicted in Fig. 4B (see the legend for the details of aligning instantaneous structures). In both the membrane-binding and solution simulations, the tips of S1 and S3 reside mainly around or between the positions of the X-ray "open" and "closed" structures. The "open" and "closed" structures share the tip position of S2, around which the S2 positions of the membrane-bound FV-C2 are distributed (Fig. 4B, left panel). The S2 positions of the solution FV-C2, on the other hand, distribute off the X-ray position: the far side from both S1 and S3 in two cases (red and black) and more closed positions to S3 (blue) in one of the simulations started with "closed" structure (Fig. 4B, right panel). The trend is attested by the Cα-RMSD of S1–S3 from the X-ray structures (Table 2). In both membrane-binding and solution simulations of FV-C2, the RMSDs of S1 and S3 from the X-ray structures are around 2–3 Å, with slightly larger values for S2. The RMSD difference of ~2–3 Å for short loops like S1–S3 (9, 7, and 8 residues were used for the calculation, respectively) may result from visibly significant structural differences to the X-ray models. One may wonder why MD-sampled structures are so different from the X-ray models? It is likely due to the difference in the crystallization and solution conditions. FVIII-C2 domain, which has ~40 % sequence similarity to FV-C2, also exhibits structural differences between the X-ray (Pratt et al., 1999) and solution structures, mainly for the regions corresponding to S1–S3 (Nuzzio et al., 2013).

Table 2
Structural deviation for membrane-bound and solution states from the X-ray "open" and "closed" conformations. The averaged Cα RMSDs of membrane-bound and solution structures from the reference structures of PDB 1CZS ("open") and 1CZV ("closed") followed by the standard deviation in parentheses. The instantaneous structures of every 0.1 ns of each simulation from the last 20 ns (membrane-bound) or 50 ns (solution) are superimposed to the reference structure using the Cα atoms of relatively stable β strands (residues 13–20 32–36, 57–61, 70–75, 85–93, 113–117, 123–127, 135–139, and 150–154). The RMSD is then calculated for the superimposed β strands (β), the whole C2 domain (All), S1 (residues 23–31), S2 (residues 40–46), and S3 (residues 76–83).

System		Membrane-bound		Solution	
Reference		1CZS ("open")	1CZV ("closed")	1CZS ("open")	1CZV ("closed")
RMSD for/Å	β	1.2 (1.0)	1.1 (1.0)	1.1 (0.5)	1.1 (0.5)
	All	2.0 (1.1)	1.9 (1.2)	2.2 (0.4)	2.1 (0.4)
	S1	2.7 (1.2)	2.0 (1.4)	3.2 (0.9)	2.1 (0.8)
	S2	2.8 (1.3)	2.8 (1.3)	3.6 (0.8)	3.7 (0.8)
	S3	2.0 (1.2)	2.5 (1.3)	2.2 (0.6)	2.7 (0.9)

3.3. Sidechain orientation of W26 shifts upon membrane binding

It has been suggested that the difference between the X-ray "open" (1CZS) and "closed" (1CZV) forms were not only due to the conformation of S1 but also the sidechain orientation of W26 and W27 (Macedo-Ribeiro et al., 1999). The relative orientation of W26 sidechain with respect to the groove enclosed by S1–S3 (the W26 opening angle) was monitored as the angle between the two vectors, one linking Cα of W26 to Cγ of W26 and the other linking Cα of W26 to Cα of L79, Fig. 5, with corresponding free-energy estimates in Fig. 6.

The average W26 opening angle for the membrane-bound FV-C2 is 56.0 ± 27.3°, which is significantly larger than that for the "closed" form (37.3°), although it is not as wide as 93.4° for the "open" form (Table 3). The W26 opening angle for FV-C2 in solution (38.7 ± 24.2°) remains close to that for the X-ray "closed". Furthermore, there are two peaks in the distribution of the W26 opening angle at around 30° and 65° (Figs. 5 and 6). In solution form of FV-C2, the former is far more populated than the latter, while in the membrane-bound form, both are equally populated. There exists, on the other hand, a single large peak in the S1–S3 distance distribution at about 13 Å (Fig. 5, left- and right-most panels; also Fig. 4), and therefore a single state with regard to the backbone of two spikes. Given that the β-barrel of FV-C2 is nearly perpendicular to the membrane surface, the observations above support that the apolar side chain of W26 in FV-C2 is kept near S1 and S3 to cover the groove between the spikes (as in the X-ray "closed" structure) in solution, and that, upon membrane binding, the sidechain changes its orientation to be inserted into the hydrophobic environment in the membrane (Fig. 3) without changing the backbone of S1 or S3.

For comparison using a complementary structural modeling approach, we generated an ensemble of hFV-C2 using the AlphaFold2 deep neural network system. The corresponding values of the W26 opening angle can be seen in Fig. 7. Notably, the ensemble closely aligns with the MD-sampled ensembles, particularly from the solution state (refer to Figs. 5 and 6). However, AlphaFold2 exclusively samples within the two distinct states defined by the boundary structures of the "closed" and "open" conformations (Fig. 7). In contract, MD simulations explore conformations mainly between these boundary states, but also extend beyond the region restricted by them. Since AlphaFold2 ignores the presence of the membrane, we suspect that the congruence between AlphaFold2 and MD ensembles reflect general conformational landscape

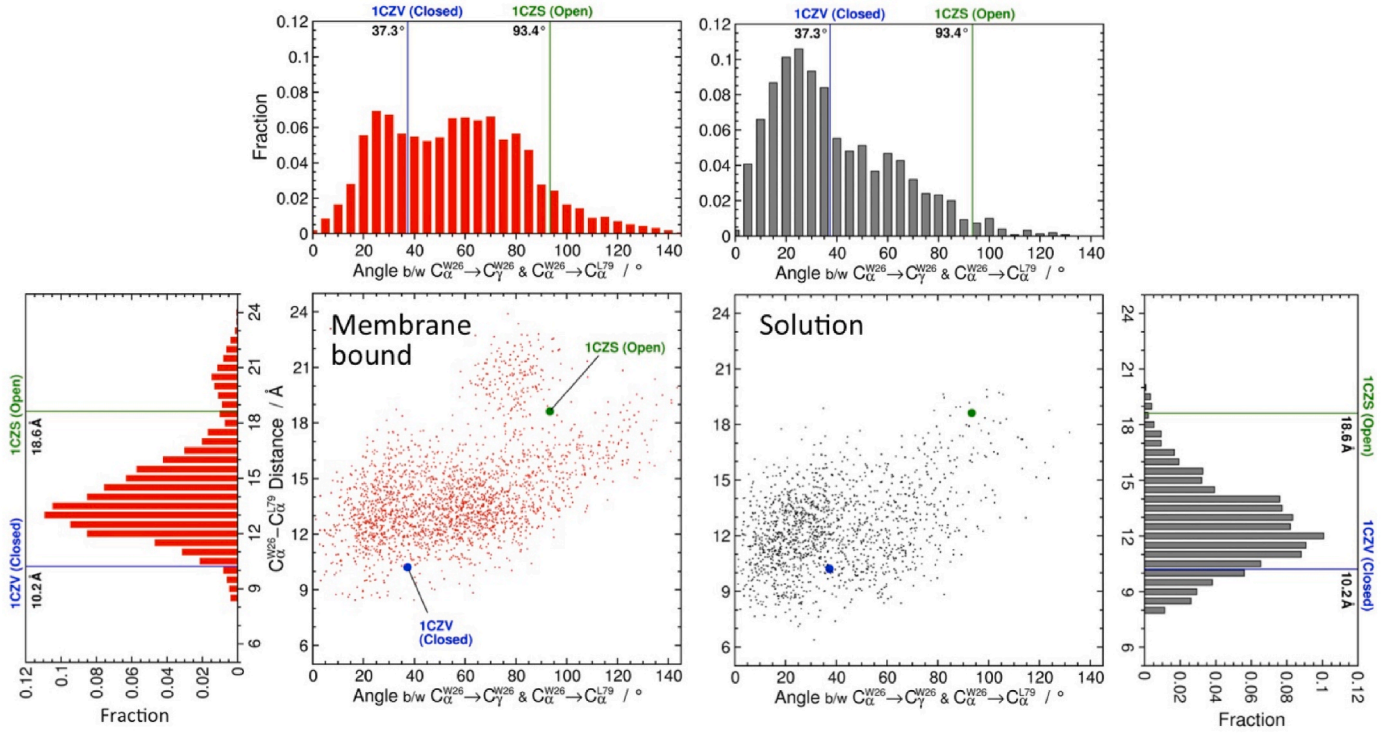

Fig. 5. Distribution of the distance between S1–S3 and W26 opening angle of membrane-bound and solution forms of FV-C2. The structures from every 0.1ns of the last 20ns from the membrane-binding simulations (Membrane bound) or 50ns from the solution simulations (Solution) are depicted in the center bottom panels as red and gray dots respectively. The W26 opening angle is to monitor the orientation of the sidechain of W26 with respect to the S1–S3, defined as the angle between the vectors W26_Cα to L79_Cα and W26_Cα to W26_Cγ. The top panels are histograms of the W26 opening angle for the same data set. The left- and right-mode panels are histograms of the S1–S3 distance. The large blue and green circles are of the X-ray structures 1CZV ("closed") and 1CZS ("open"), respectively, whose distances and angles are also indicated on the histograms using the same colors.

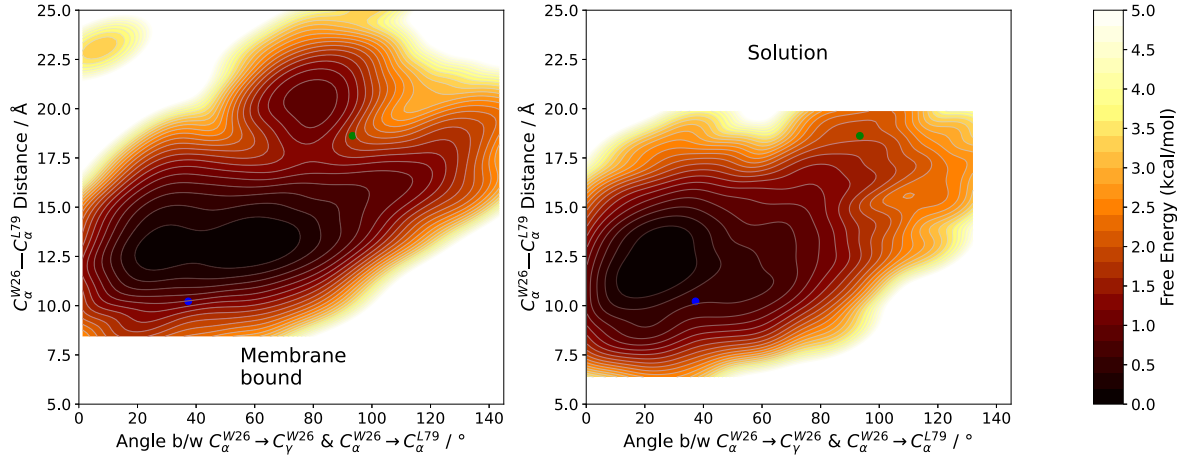

Fig. 6. Free-energy estimates from the distribution of the distance between S1–S3 and W26 opening angle of membrane-bound and solution forms of FV-C2. The data corresponds to those presented in Fig. 5, with the free energy being estimated according to the equation $\overline{F}_i = -k_B T \ln P_i$, where P_i is the 2D-Gaussian kernel density estimate of points. Identical contour-level spacing are used in the two panels, set at 0.2 kcal/mol. The large blue and green circles are of the X-ray structures 1CZV ("closed") and 1CZS ("open"), respectively.

of FV-C2, whereas the membrane-bound ensemble from MD reveals the adaptation upon binding the membrane.

3.4. A PS headgroup moiety binding to the PS-specificity pocket

A putative PS-specificity pocket composed of K23, Q48, and S78 of FV-C2 was previously proposed, based on the crystal structure (Macedo-Ribeiro et al., 1999) (Fig. 1). A PS lipid may be tucked into the pocket and its headgroup moieties would establish hydrogen bonds: the carboxy moiety with Q48 carboxamide and S78 hydroxy groups, as well as the phosphate moiety with K23 ε-amino group. The membrane-binding simulations captured binding of a PS headgroup to the PS-specificity pocket of FV-C2 repeatedly. In 8 out of 9 simulations, however, the pattern of the hydrogen bonds was different from that in the originally proposed model (Macedo-Ribeiro et al., 1999), with the PS phosphate moiety interacting with S78 and the carboxy with K23 (Fig. 8). The amino moiety occasionally interacts with Q48, but the moiety is often pointing towards the membrane and away from S2.

Table 3
Average Spike 1–Spike 3 distance and W26 opening angle. The averages of the Spike 1 - Spike 3 distance (defined as the distance between W26_Cα and L79_Cα) and of the opening angle of the W26 sidechain (defined as the angle between the vectors W26_Cα to L79_Cα and W26_Cα to W26_Cγ) for the systems listed in Table 1, with the standard deviation in parentheses. The distances and angles for the reference "closed" (PDB 1CZV) and "open" (1CZS) structures are also listed.

System	Init. Conformation	S1–S3 distance/ Å	W26 opening angle/°
Membrane	"closed"	14.2 (2.6)	56.0 (27.3)
Solution	All	12.4 (2.2)	38.7 (24.2)
	"closed"	12.5 (2.5)	51.7 (28.4)
	"open"	12.3 (2.0)	32.2 (18.6)
1CZV ("closed")	–	10.2	37.3
1CZS ("open")	–	18.6	93.4

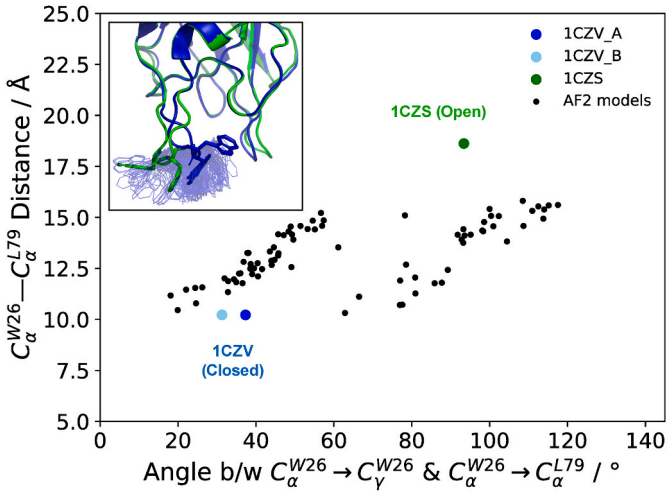

Fig. 7. Distribution of the distance between S1–S3 and W26 opening angle of AlphaFold2-predicted FV-C2 conformations. The large blue and green circles are of the X-ray structures 1CZV ("closed") and 1CZS ("open"), respectively. The insert shows the X-ray structures 1CZV ("closed", in blue) and 1CZS ("open", in green) in cartoon representation, respectively, with the AlphaFold2 ensemble indicated by showing the W26 and W27 orientations (in translucent licorice representation).

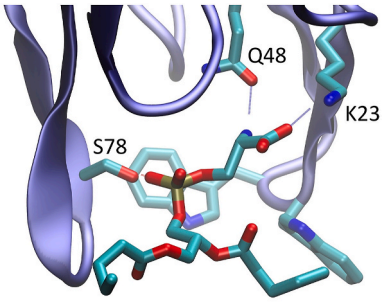

Fig. 8. Identifying the PS-specificity pocket. A snapshot of a PS lipid (depicted in licorice representation) from one of the membrane-binding simulations is shown. The lipid resides in the PS-specificity pocket, interacting with K23, Q48, and S78. The backbone of the C2 domain is shown as blue tubes and the sidechain of K23, Q48 and S78 are in licorice representation.

If this binding pattern of a single PS to the pocket is essential to the membrane binding of FV-C2, a speculation could be made on a membrane binding of FV-C2, just like the "Anything But Choline" (ABC) hypothesis for GLA domain (Tavoosi et al., 2011; Tavoosi and Morrissey, 2013, Tavoosi et al., 2013). Since both phosphate and carboxy moieties from a single lipid need to interact with S78 and K23 of FV-C2, respectively, lipids with a small headgroup such as phosphatidic acid (PA) probably cannot bind to the pocket stably. On the other hand, a lipid with a phosphatidylethanolamine (PE) headgroup may be able to bind to the pocket at its phosphate interacting with S78 and at the amino group with Q48 but without interacting with K23 (which was not observed in membrane-binding simulation). In a similar manner, other lipids like sphingomyelin or phosphatidylcholine might also be able to bind the pocket weakly, and perhaps even cholesterol could play a role (Banerjee and Sen, 2023, Javanainen et al., 2023). These speculations would lead to a potential rule that "anything but PA" may be able to bind the pocket, albeit with somewhat lower affinities.

FV-C2 contains both hydrophobic residues (e.g., W26 and W27 on S1) and basic residues (e.g., K23, K24 on S1 and R43 on S2). It is thus expected that membrane binding of FV-C2 is based on nonspecific hydrophobic contacts between the nonpolar residues, the acyl tails, and more specific electrostatic contacts between the basic residues and anionic headgroups (including the PS-specificity pocket). Average numbers of lipid atoms in contact with individual residues are shown for

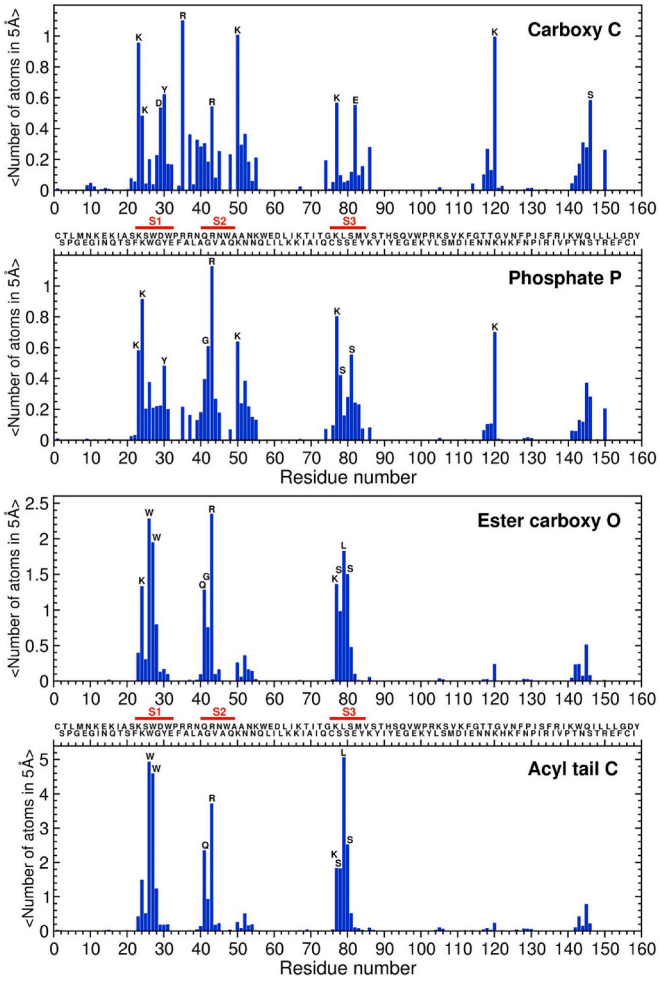

Fig. 9. Interaction between PS lipids and FV-C2 sidechains. For each residue of FV-C2, the expected numbers of interacting lipid moieties, defined as the average numbers of moieties within 5 Å are plotted for carboxy carbon (top panel), phosphorus (second top), ester carboxy oxygen (second bottom), and acyl tail carbon (bottom) atoms. 200 instantaneous structures from every 0.1ns out of the last 20 ns (i.e., 30–50ns duration) of the twelve membrane-binding simulations were used for the computation (see also Table 1). The sequence of FV-C2 is shown in the middle along the residue number, with the regions of S1–S3 indicated by red bars and labels. The bars exceeding 0.5 are also labeled with the amino acid code.

the membrane-bound FV-C2 in Fig. 9. All K and R residues near or on S1 and S3 and K120 are in contact with phosphosphate and/or carboxy groups of PS headgroups with relatively larger (>0.6) counts, whereas apolar residues (e.g., W26 and W27 on S1; L79 on S3) are mainly in contact with the glycerol and acyl tail layer.

In the S1–S3 distance distribution for the membrane-bound FV-C2, there is a hump centered around 20 Å which is not observed the in the solution form (Fig. 5). This is contributed from a single trajectory (the outlier line in the top-left, "membrane S1–S3" plot of Fig. 4A). The observed "open"-like state in the trajectory, however, is different from the 1CZS structure (Macedo-Ribeiro et al., 1999). One of the noticeable differences is the dislocation in the backbone segment of residues 44–56. We note, however, such a structure was observed only in one out of twelve trajectories, and that we currently cannot judge if the structure could be an artifact.

3.5. Comparison with FVIII-C2

FV-C2 has high similarity to FVIII-C2 both in sequence (Fig. 2) and structure (Ngo et al., 2008). It is hence expected that FVIII-C2 would bind to anionic membranes with a similar insertion depth and orientation to FV-C2 as suggested previously (Pratt et al., 1999). The membrane-bound form of the homologous FVIII-C2 has been proposed implicitly in a study on the intrinsic factor Xase binary complex to be positioned with the β-barrel of FVIII-C2 to be heavily inclined relative to the membrane surface (so was the juxtaposed FVIII-C1) (Pratt et al., 1999). Since FV-C2 and FVIII-C2 exhibit strong similarities in their membrane-binding mode (Madsen et al., 2015), the suggestion would follow what that the tilted or inclined orientation of FVIII (Wakabayashi and Fay, 2013) likely stems from preferred orientation of C1 and not C2 because the latter prefers the upright orientation (see Fig. 3 above and Fig. 4 of (Madsen et al., 2015)). In addition, the detailed lipid interactions of FV-C2 and FVIII-C2 are not identical, which raises questions regarding different mechanisms for their membrane binding and lipid specificities. In fact, our results are in excellent overall agreement with recently published works using similar methodology on homologous C2 domains, including lactadherin-C2 and FVIII-C2 (Madsen et al., 2015; De Lio et al., 2020; Li et al., 2022; Cheng et al., 2023; Ohkubo and Madsen, 2023) but we note that it appears that the PS-specificity pockets among these domains are not identical, nor do they appear to bind PS moieties with the same interaction pattern.

For FV-C2, it was often observed in the membrane-binding simulations that a PS headgroup interacts with K23 at the carboxy group, Q48 at the phosphate and carboxy, and S78 at the phosphate group. This hydrogen bond pattern is different from the previously postulated based on the X-ray "open" structure (Macedo-Ribeiro et al., 1999). In FVIII-C2, F2196, R2220, and S2250 correspond to these K23, Q48, and S78 of FV-C2 (Fig. 2). If FVIII-C2 binds to the membrane, exhibiting a similar insertion depth and orientation to FV-C2, a PS headgroup may also bind to the "pocket" among the spikes of FVIII-C2. The phosphate group of the headgroup may interact with S2250, and the carboxy group can contact R2220, which should be easier to reach than Q48 in FV-C2 due to its longer side chain. However, our previous investigation showed that not only R2220 but also R2320 is available to make contact with the lipid carboxy group (Madsen et al., 2015). The more accessible and multiple residues may be one of the reasons why FVIII-C2 has higher binding affinity to PS-containing vesicles than FV-C2 (Gilbert et al., 2012). The affinity measurement for the wild-type FV-C2 and FVIII-C2 and their point mutants on the "pocket"-forming residues under the same condition would be able to substantiate our results and speculations.

4. Conclusions

Establishing accurate membrane-bound models for the membrane-binding domains (i.e., the C2 and GLA domains) of coagulation factors is crucial for elucidating the molecular mechanisms underlying these components' association and function on the membrane surface. We have repeatedly and consistently observed spontaneous membrane binding of FV-C2, facilitating the development of reliable membrane-bound models of FV-C2, exploration of membrane-induced conformational dynamics and identification of specific lipid–protein interactions. In its bound state, FV-C2 exhibits a configuration with spikes 1–3 about 10 Å inserted below the membrane surface, and the β-barrel oriented nearly normal to the membrane surface. Upon binding, the hydrophobic residue W26 becomes more exposed to the acyl tails of the membrane lipids, while the backbone structures of spikes 1 and 3 undergo minimal changes. A PS headgroup was observed to interact with basic or polar residues at the previously postulated PS-specificity pocket, but in a different interaction pattern. Despite existing crystal structures representing presumed "open" and "closed" states of FV-C2, our results revealed a continuous distribution of structures between these states, with the most populated structures differing from both "open" and "closed" states observed in crystal environments. Structural prediction with AlphaFold2 is consistent with these observations. Our results form a framework for refining putative models of FV and FVIII, and consequently, membrane-bound PTase and intrinsic FXase complexes, suggesting potential experiments such as mutagenesis studies to further validate and enhance our understanding of these membrane-bound proteins and complexes.

CRediT authorship contribution statement

Y. Zenmei Ohkubo: Conceptualization, Methodology, Formal analysis, Investigation, Visualization, Writing – original draft, Writing – review & editing. **Peter W. Radulovic:** Investigation, Writing – review & editing. **Albert N. Kahira:** Investigation, Writing – review & editing. **Jesper J. Madsen:** Conceptualization, Investigation, Visualization, Writing – original draft, Writing – review & editing.

Declaration of competing interest

The authors declare that they have no known competing financial interests or personal relationships that could have appeared to influence the work reported in this paper.

Data availability

Data will be made available on request.

Acknowledgements

Simulations were performed using XSEDE resources (grant number MCA06N060) and the Advanced Computing Resources at University of South Florida. Special thanks are given to the Illinois Hemostasis Group members (especially Emad Tajkhorshid, James H. Morrissey and Chad M. Rienstra) for many stimulating discussions and establishing the environment where the work presented in this article initiated. Giray Enkavi is thanked for technical assistance.

References

Adams, T.E., Hockin, M.F., Mann, K.G., Everse, S.J., 2004. The crystal structure of activated protein C-inactivated bovine factor Va: implications for cofactor function. Proc. Natl. Acad. Sci. U.S.A. 101 (24), 8918–8923.

Antila, H., Buslaev, P., Favela-Rosales, F., Ferreira, T.M., Gushchin, I., Javanainen, M., Kav, B., Madsen, J.J., Melcr, J., Miettinen, M.S., Maatta, J., Nencini, R., Ollila, O.H. S., Piggot, T.J., 2019. Headgroup structure and cation binding in phosphatidylserine lipid bilayers. J. Phys. Chem. B 123 (43), 9066–9079.

Arcario, M.J., Ohkubo, Y.Z., Tajkhorshid, E., 2011. Capturing spontaneous partitioning of peripheral proteins using a biphasic membrane-mimetic model. J. Phys. Chem. B 115 (21), 7029–7037.

Bacle, A., Buslaev, P., Garcia-Fandino, R., Favela-Rosales, F., Mendes Ferreira, T., Fuchs, P.F.J., Gushchin, I., Javanainen, M., Kiirikki, A.M., Madsen, J.J., Melcr, J., Milan Rodriguez, P., Miettinen, M.S., Ollila, O.H.S., Papadopoulos, C.G., Peon, A.,

Piggot, T.J., Pineiro, A., Virtanen, S.I., 2021. Inverse conformational selection in lipid-protein binding. J. Am. Chem. Soc. 143 (34), 13701–13709.
Banerjee, S., Sen, P., 2023. A molecular dynamics simulation study to understand the effect of cholesterol and tissue factor palmitoylation on tissue factor-factor VIIa-factor Xa ternary complex in different lipid environments. J. Thromb. Haemostasis 21 (4), 917–932.
Baumgartner, S., Hofmann, K., Chiquet-Ehrismann, R., Bucher, P., 1998. The discoidin domain family revisited: new members from prokaryotes and a homology-based fold prediction. Protein Sci. 7 (7), 1626–1631.
Baylon, J.L., Vermaas, J.V., Muller, M.P., Arcario, M.J., Pogorelov, T.V., Tajkhorshid, E., 2016. Atomic-level description of protein-lipid interactions using an accelerated membrane model. Biochim. Biophys. Acta 1858 (7 Pt B), 1573–1583.
Boettcher, J.M., Davis-Harrison, R.L., Clay, M.C., Nieuwkoop, A.J., Ohkubo, Y.Z., Tajkhorshid, E., Morrissey, J.H., Rienstra, C.M., 2011. Atomic view of calcium-induced clustering of phosphatidylserine in mixed lipid bilayers. Biochemistry 50 (12), 2264–2273.
Bos, M.H., Camire, R.M., 2010. Blood coagulation factors V and VIII: molecular mechanisms of procofactor activation. J. Coagul. Disord. 2 (2), 19–27.
Cheng, K.V., De Lio, A.M., Jain, R., Paul, D., Morrissey, J.H., Pogorelov, T.V., 2023. Lactadherin's multistate binding predicts stable membrane-bound conformations of factors V and VIII's C domains. Biochemistry 62 (20), 3020–3032.
Darden, T., York, D., Pedersen, L., 1993. Particle mesh Ewald - an N.Log(N) method for Ewald sums in large systems. J. Chem. Phys. 98 (12), 10089–10092.
De Lio, A.M., Paul, D., Jain, R., Morrissey, J.H., Pogorelov, T.V., 2020. Proteins and ions compete for membrane interaction: the case of lactadherin. https://www.biorxiv.org/content/10.1101/2020.04.03.023838v2.
Di Cera, E., Mohammed, B.M., Pelc, L.A., Stojanovski, B.M., 2022. Cryo-EM structures of coagulation factors. Res Pract Thromb Haemost 6 (7), e12830.
Essmann, U., Perera, L., Berkowitz, M.L., Darden, T., Lee, H., Pedersen, L.G., 1995. A smooth particle mesh Ewald method. J. Chem. Phys. 103 (19), 8577–8593.
Feller, S.E., Zhang, Y.H., Pastor, R.W., Brooks, B.R., 1995. Constant-pressure molecular-dynamics simulation - the Langevin piston method. J. Chem. Phys. 103 (11), 4613–4621.
Gilbert, G.E., Novakovic, V.A., Kaufman, R.J., Miao, H.Z., Pipe, S.W., 2012. Conservative mutations in the C2 domains of factor VIII and factor V alter phospholipid binding and cofactor activity. Blood 120 (9), 1923–1932.
Hestenes, M.R., Stiefel, E., 1952. Methods of conjugate gradients for solving linear systems. J. Res. Natl. Bur. Stand. 49 (6), 409–436.
Javanainen, M., Heftberger, P., Madsen, J.J., Miettinen, M.S., Pabst, G., Ollila, O.H.S., 2023. Quantitative comparison against experiments reveals imperfections in force fields' descriptions of POPC-cholesterol interactions. J. Chem. Theor. Comput. 19 (18), 6342–6352.
Jorgensen, W.L., Chandrasekhar, J., Madura, J.D., Impey, R.W., Klein, M.L., 1983. Comparison of simple potential functions for simulating liquid water. J. Chem. Phys. 79 (2), 926–935.
Jumper, J., Evans, R., Pritzel, A., Green, T., Figurnov, M., Ronneberger, O., Tunyasuvunakool, K., Bates, R., Zidek, A., Potapenko, A., Bridgland, A., Meyer, C., Kohl, S.A.A., Ballard, A.J., Cowie, A., Romera-Paredes, B., Nikolov, S., Jain, R., Adler, J., Back, T., Petersen, S., Reiman, D., Clancy, E., Zielinski, M., Steinegger, M., Pacholska, M., Berghammer, T., Bodenstein, S., Silver, D., Vinyals, O., Senior, A.W., Kavukcuoglu, K., Kohli, P., Hassabis, D., 2021. Highly accurate protein structure prediction with AlphaFold. Nature 596 (7873), 583.
Kiirikki, A.M., Antila, H.S., Bort, L.S., Buslaev, P., Favela-Rosales, F., Ferreira, T.M., Fuchs, P.F.J., Garcia-Fandino, R., Gushchin, I., Kav, B., Kucerka, N., Kula, P., Kurki, M., Kuzmin, A., Lalitha, A., Lolicato, F., Madsen, J.J., Miettinen, M.S., Mingham, C., Monticelli, L., Nencini, R., Nesterenko, A.M., Piggot, T.J., Piñeiro, A., Reuter, N., Samantray, S., Suárez-Lestón, F., Talandashti, R., Ollila, O.H.S., 2024. Overlay databank unlocks data-driven analyses of biomolecules for all. Nat. Commun. 15 (1).
Larkin, M.A., Blackshields, G., Brown, N.P., Chenna, R., McGettigan, P.A., McWilliam, H., Valentin, F., Wallace, I.M., Wilm, A., Lopez, R., Thompson, J.D., Gibson, T.J., Higgins, D.G., 2007. Clustal W and clustal X version 2.0. Bioinformatics 23 (21), 2947–2948.
Lechtenberg, B.C., Murray-Rust, T.A., Johnson, D.J., Adams, T.E., Krishnaswamy, S., Camire, R.M., Huntington, J.A., 2013. Crystal structure of the prothrombinase complex from the venom of Pseudonaja textilis. Blood 122 (16), 2777–2783.
Lemmon, M.A., 2008. Membrane recognition by phospholipid-binding domains. Nat. Rev. Mol. Cell Biol. 9 (2), 99–111.
Li, J., Chen, H., Liu, S., Kang, Z., Yu, L., Liang, L., Shen, J.W., Liu, Y., Fan, J., Wang, Q., 2022. Understanding the anchoring interaction of coagulation factor Va light chain on zeolites: a molecular dynamics study. J. Colloid Interface Sci. 608 (Pt 1), 435–445.
Lin, L., Huai, O., Huang, M.D., Furie, B., Furie, B.C., 2007. Crystal structure of the bovine lactadherin C2 domain, a membrane binding motif, shows similarity to the C2 domains of factor V and factor VIII. J. Mol. Biol. 371 (3), 717–724.
Macedo-Ribeiro, S., Bode, W., Huber, R., Quinn-Allen, M.A., Kim, S.W., Ortel, T.L., Bourenkov, G.P., Bartunik, H.D., Stubbs, M.T., Kane, W.H., Fuentes-Prior, P., 1999. Crystal structures of the membrane-binding C2 domain of human coagulation factor V. Nature 402 (6760), 434–439.
MacKerell, A.D., Bashford, D., Bellott, M., Dunbrack, R.L., Evanseck, J.D., Field, M.J., Fischer, S., Gao, J., Guo, H., Ha, S., Joseph-McCarthy, D., Kuchnir, L., Kuczera, K., Lau, F.T.K., Mattos, C., Michnick, S., Ngo, T., Nguyen, D.T., Prodhom, B., Reiher, W. E., Roux, B., Schlenkrich, M., Smith, J.C., Stote, R., Straub, J., Watanabe, M., Wiórkiewicz-Kuczera, J., Yin, D., Karplus, M., 1998. All-atom empirical potential for molecular modeling and dynamics studies of proteins. J. Phys. Chem. B 102 (18), 3586–3616.
Mackerell, A.D., Feig, M., Brooks, C.L., 2004. Extending the treatment of backbone energetics in protein force fields: limitations of gas-phase quantum mechanics in reproducing protein conformational distributions in molecular dynamics simulations. J. Comput. Chem. 25 (11), 1400–1415.
Madsen, J.J., Ohkubo, Y.Z., Peters, G.H., Faber, J.H., Tajkhorshid, E., Olsen, O.H., 2015. Membrane interaction of the factor VIIIa discoidin domains in atomistic detail. Biochemistry 54 (39), 6123–6131.
Majumder, R., Quinn-Allen, M.A., Kane, W.H., Lentz, B.R., 2005. The phosphatidylserine binding site of the factor Va C2 domain accounts for membrane binding but does not contribute to the assembly or activity of a human factor X-factor V complex. Biochemistry 44 (2), 711–718.
Majumder, R., Quinn-Allen, M.A., Kane, W.H., Lentz, B.R., 2008. A phosphatidylserine binding site in factor V C1 domain regulates both assembly and activity of the prothrombinase complex. Blood 112 (7), 2795–2802.
Martyna, G.J., Tobias, D.J., Klein, M.L., 1994. Constant-pressure molecular-dynamics algorithms. J. Chem. Phys. 101 (5), 4177–4189.
Mirdita, M., Schutze, K., Moriwaki, Y., Heo, L., Ovchinnikov, S., Steinegger, M., 2022. ColabFold: making protein folding accessible to all. Nat. Methods 19 (6), 679.
Mohammed, B.M., Pelc, L.A., Rau, M.J., Di Cera, E., 2023. Cryo-EM structure of coagulation factor V short. Blood 141 (26), 3215–3225.
Mollica, L., Fraternali, F., Musco, G., 2006. Interactions of the C2 domain of human Factor V with a model membrane. Proteins: Struct., Funct., Bioinf. 64 (2), 363–375.
Nalefski, E.A., Falke, J.J., 1996. The C2 domain calcium-binding motif: structural and functional diversity. Protein Sci. 5 (12), 2375–2390.
Ngo, J.C.K., Huang, M., Roth, D.A., Furie, B.C., Furie, B., 2008. Crystal structure of human factor VIII: implications for the formation of the factor IXa-factor VIIIa complex. Structure 16 (4), 597–606.
Nicolaes, G.A.F., Villoutreix, B.O., Dahlbäck, B., 2000. Mutations in a potential phospholipid binding loop in the C2 domain of factor V affecting the assembly of the prothrombinase complex. Blood Coagul. Fibrinolysis 11 (1), 89–100.
Nuzzio, K.M., Cullinan, D.B., Novakovic, V.A., Boettcher, J.M., Rienstra, C.M., Gilbert, G. E., Baleja, J.D., 2013. Backbone resonance assignments of the C2 domain of coagulation factor VIII. Biomolecular Nmr Assignments 7 (1), 31–34.
Ohkubo, Y.Z., Madsen, J.J., 2021. Uncovering membrane-bound models of coagulation factors by combined experimental and computational approaches. Thromb. Haemostasis 121 (9), 1122–1137.
Ohkubo, Y.Z., Madsen, J.J., 2023. Elucidating the complex membrane binding of a protein with multiple anchoring domains. https://www.biorxiv.org/content/10.1101/2023.08.10.552738v1.abstract.
Ohkubo, Y.Z., Pogorelov, T.V., Arcario, M.J., Christensen, G.A., Tajkhorshid, E., 2012. Accelerating membrane insertion of peripheral proteins with a novel membrane mimetic model. Biophys. J. 102 (9), 2130–2139.
Ohkubo, Y.Z., Tajkhorshid, E., 2008. Distinct structural and adhesive roles of Ca in membrane binding of blood coagulation factors. Structure 16 (1), 72–81.
Ortel, T.L., Devorecarter, D., Quinnallen, M.A., Kane, W.H., 1992a. Deletion analysis of recombinant human factor-V - evidence for a phosphatidylserine binding-site in the 2nd C-type domain. J. Biol. Chem. 267 (6), 4189–4198.
Ortel, T.L., Quinnallen, M.A., Charles, L.A., Devorecarter, D., Kane, W.H., 1992b. Characterization of an acquired inhibitor to coagulation factor-V - antibody-binding to the 2nd C-type domain of factor-V inhibits the binding of factor-V to phosphatidylserine and neutralizes procoagulant activity. J. Clin. Invest. 90 (6), 2340–2347.
Pellequer, J.L., Gale, A.J., Getzoff, E.D., Griffin, J.H., 2000. Three-dimensional model of coagulation factor Va bound to activated protein C. Thromb. Haemostasis 84 (5), 849–857.
Pellequer, J.L., Gale, A.J., Griffin, J.H., Getzoff, E.D., 1998. Homology models of the C domains of blood coagulation factors V and VIII: a proposed membrane binding mode for FV and FVIII C2 domains. Blood Cells Mol. Dis. 24 (4), 448–461.
Peng, W., Quinn-Allen, M.A., Kane, W.H., 2005. Mutation of hydrophobic residues in the factor Va C1 and C2 domains blocks membrane-dependent prothrombin activation. J. Thromb. Haemostasis 3 (2), 351–354.
Perisic, O., Fong, S., Lynch, D.E., Bycroft, M., Williams, R.L., 1998. Crystal structure of a calcium-phospholipid binding domain from cytosolic phospholipase A2. J. Biol. Chem. 273 (3), 1596–1604.
Petrache, H.I., Tristram-Nagle, S., Gawrisch, K., Harries, D., Parsegian, V.A., Nagle, J.F., 2004. Structure and fluctuations of charged phosphatidylserine bilayers in the absence of salt. Biophys. J. 86 (3), 1574–1586.
Phillips, J.C., Braun, R., Wang, W., Gumbart, J., Tajkhorshid, E., Villa, E., Chipot, C., Skeel, R.D., Kalé, L., Schulten, K., 2005. Scalable molecular dynamics with NAMD. J. Comput. Chem. 26 (16), 1781–1802.
Pratt, K.P., Shen, B.W., Takeshima, K., Davie, E.W., Fujikawa, K., Stoddard, B.L., 1999. Structure of the C2 domain of human factor VIII at 1.5 A resolution. Nature 402 (6760), 439–442.
Rietveld, I.M., Bos, M.H.A., Lijfering, W.M., Li-Gao, R.F., Rosendaal, F.R., Reitsma, P.H., Cannegieter, S.C., 2018. Factor V levels and risk of venous thrombosis: the MEGA case-control study. Research and Practice in Thrombosis and Haemostasis 2 (2), 320–326.
Rizo, J., Südhof, T.C., 1998. C-domains, structure and function of a universal Ca-binding domain. J. Biol. Chem. 273 (26), 15879–15882.
Ruben, E.A., Rau, M.J., Fitzpatrick, J.A.J., Di Cera, E., 2021. Cryo-EM structures of human coagulation factors V and Va. Blood 137 (22), 3137–3144.
Ruben, E.A., Summers, B., Rau, M.J., Fitzpatrick, J.A.J., Di Cera, E., 2022. Cryo-EM structure of the prothrombin-prothrombinase complex. Blood 139 (24), 3463–3473.
Schreuder, M., Reitsma, P.H., Bos, M.H.A., 2019. Blood coagulation factor Va's key interactive residues and regions for prothrombinase assembly and prothrombin binding. J. Thromb. Haemostasis 17 (8), 1229–1239.

Segers, K., Sperandio, O., Sack, M., Fischer, R., Miteva, M.A., Rosing, J., Nicolaes, G.A.F., Villoutreix, B.O., 2007. Design of protein-membrane interaction inhibitors by virtual ligand screening, proof of concept with the C2 domain of factor V. Proc. Natl. Acad. Sci. U.S.A. 104 (31), 12697–12702.

Shao, C., Novakovic, V.A., Head, J.F., Seaton, B.A., Gilbert, G.E., 2008. Crystal structure of lactadherin C2 domain at 1.7A resolution with mutational and computational analyses of its membrane-binding motif. J. Biol. Chem. 283 (11), 7230–7241.

Shen, B.W., Spiegel, P.C., Chang, C.H., Huh, J.W., Lee, J.S., Kim, J., Kim, Y.H., Stoddard, B.L., 2008. The tertiary structure and domain organization of coagulation factor VIII. Blood 111 (3), 1240–1247.

Spiegel, P.C., Jacquemin, M., Saint-Remy, J.M.R., Stoddard, B.L., Pratt, K.P., 2001. Structure of a factor VIIIC2 domain-immunoglobulin G4κ Fab complex:: identification of an inhibitory antibody epitope on the surface of factor VIII. Blood 98 (1), 13–19.

Spiegel, P.C., Murphy, P., Stoddard, B.L., 2004. Surface-exposed hemophilic mutations across the factor VIIIC2 domain have variable effects on stability and binding activities. J. Biol. Chem. 279 (51), 53691–53698.

Srivastava, A., Quinn-Allen, M.A., Kim, S.W., Kane, W.H., Lentz, B.R., 2001. Soluble phosphatidylserine binds to a single identified site in the C2 domain of human factor V. Biochemistry 40 (28), 8246–8255.

Stace, C.L., Ktistakis, N.T., 2006. Phosphatidic acid- and phosphatidylserine-binding proteins. Biochim. Biophys. Acta Mol. Cell Biol. Lipids 1761 (8), 913–926.

Steinegger, M., Soding, J., 2017. MMseqs2 enables sensitive protein sequence searching for the analysis of massive data sets. Nat. Biotechnol. 35 (11), 1026–1028.

Stoilova-Mcphie, S., Parmenter, C.D.J., Segers, K., Villoutreix, B.O., Nicolaes, G.A.F., 2008. Defining the structure of membrane-bound human blood coagulation factor Va. J. Thromb. Haemostasis 6 (1), 76–82.

Sunnerhagen, M., Forsen, S., Hoffren, A.M., Drakenberg, T., Teleman, O., Stenflo, J., 1995. Structure of the Ca2+-free gla domain sheds light on membrane-binding of blood-coagulation proteins. Nat. Struct. Biol. 2 (6), 504–509.

Svensson, L.A., Thim, L., Olsen, O.H., Nicolaisen, E.M., 2013. Evaluation of the metal binding sites in a recombinant coagulation factor VIII identifies two sites with unique metal binding properties. Biol. Chem. 394 (6), 761–765.

Tavoosi, N., Davis-Harrison, R.L., Pogorelov, T.V., Ohkubo, Y.Z., Arcario, M.J., Clay, M. C., Rienstra, C.M., Tajkhorshid, E., Morrissey, J.H., 2011. Molecular determinants of phospholipid synergy in blood clotting. J. Biol. Chem. 286 (26), 23247–23253.

Tavoosi, N., Morrissey, J.H., 2013. Surprising phospholipid specificity of two blood clotting proteins: factor VII and protein C. Faseb. J. 27.

Tavoosi, N., Smith, S.A., Davis-Harrison, R.L., Morrissey, J.H., 2013. Factor VII and protein C are phosphatidic acid-binding proteins. Biochemistry 52 (33), 5545–5552.

Vanommeslaeghe, K., Hatcher, E., Acharya, C., Kundu, S., Zhong, S., Shim, J., Darian, E., Guvench, O., Lopes, P., Vorobyov, I., MacKerell, A.D., 2010. CHARMM general force field: a force field for drug-like molecules compatible with the CHARMM all-atom additive biological force fields. J. Comput. Chem. 31 (4), 671–690.

Verdaguer, N., Corbalan-Garcia, S., Ochoa, W.F., Fita, I., Gómez-Fernández, J.C., 1999. Ca2+ bridges the C2 membrane-binding domain of protein kinase Cα directly to phosphatidylserine. EMBO J. 18 (22), 6329–6338.

Vermaas, J.V., Baylon, J.L., Arcario, M.J., Muller, M.P., Wu, Z., Pogorelov, T.V., Tajkhorshid, E., 2015. Efficient exploration of membrane-associated phenomena at atomic resolution. J. Membr. Biol. 248 (3), 563–582.

Vermaas, J.V., Pogorelov, T.V., Tajkhorshid, E., 2017. Extension of the highly mobile membrane mimetic to transmembrane systems through customized in silico solvents. J. Phys. Chem. B 121 (15), 3764–3776.

Villoutreix, B.O., Bucher, P., Hofmann, K., Baumgartner, S., Dahlback, B., 1998. Molecular models for the two discoidin domains of human blood coagulation factor V. J. Mol. Model. 4 (8), 268–275.

Wakabayashi, H., Fay, P.J., 2013. Molecular orientation of factor VIIIa on the phospholipid membrane surface determined by fluorescence resonance energy transfer. Biochem. J. 452 (2), 293–301.

Wu, S., Lee, C.J., Pedersen, L.G., 2009. Conformational change path between closed and open forms of C2 domain of coagulation factor V on a two-dimensional free-energy surface. Phys. Rev. 79 (4).

Zwaal, R.F., Comfurius, P., Bevers, E.M., 1998. Lipid-protein interactions in blood coagulation. Biochim. Biophys. Acta 1376 (3), 433–453.